*electrochem*

MDPI

*Article*

# Influence of Pulsed Reverse Electrodeposition on Mechanical Properties of Ni–W Alloys

**Zeyu Gu [1], Jhen-Yang Wu [1,*], Yiming Jiang [1], Tomoyuki Kurioka [1], Chun-Yi Chen [1], Hwai-En Lin [2], Xun Luo [3], Daisuke Yamane [4], Masato Sone [1] and Tso-Fu Mark Chang [1,*]**

1 Institute of Innovative Research, Tokyo Institute of Technology, Yokohama 226-8503, Japan; gu.z.ad@m.titech.ac.jp (Z.G.); jiang@ames.pi.titech.ac.jp (Y.J.); kurioka.t.aa@m.titech.ac.jp (T.K.); chen.c.ac@m.titech.ac.jp (C.-Y.C.); sone.m.aa@m.titech.ac.jp (M.S.)
2 Department of Mechanical Engineering, National Taipei University of Technology, Taipei 106344, Taiwan; linhe@ntut.edu.tw
3 Key Laboratory of Light Metal Materials Processing Technology of Guizhou Province, Guizhou Institute of Technology, Guiyang 550003, China; cloudlx@163.com
4 Department of Mechanical Engineering, Ritsumeikan University, Kusatsu, Shiga 525-8577, Japan; dyamane@fc.ritsumei.ac.jp
* Correspondence: wu.j.ar@m.titech.ac.jp (J.-Y.W.); chang.m.aa@m.titech.ac.jp (T.-F.M.C.)

**Abstract:** Ni–W alloys have received considerable interest as a promising structural material for microelectromechanical systems (MEMS) due to their exceptional properties, including hardness, ductility, corrosion resistance, and thermal stability. However, the electrodeposition of Ni–W alloys in the MEMS fabrication process to achieve intact structures with a thickness of several tens of micrometers is challenging due to the occurrence of cracking caused by side reactions and internal stresses during the electrodeposition process. To address this issue, our focus was on pulsed reverse electrodeposition (PRE) as a potential solution. The utilization of the PRE technique allows for a high concentration of reactive species on the electrode surface, thereby mitigating side reactions such as hydrogen generation. In this study, we examined the effects of the PRE method on the morphological characteristics, average crystal grain size, Vickers hardness, and micro-mechanical properties of Ni–W alloys.

**Keywords:** Ni–W alloy; pulsed reverse electrodeposition; micro-mechanical properties; Vickers hardness; MEMS



**Citation:** Gu, Z.; Wu, J.-Y.; Jiang, Y.; Kurioka, T.; Chen, C.-Y.; Lin, H.-E.; Luo, X.; Yamane, D.; Sone, M.; Chang, T.-F.M. Influence of Pulsed Reverse Electrodeposition on Mechanical Properties of Ni–W Alloys. *Electrochem* **2024**, *5*, 287–297. https://doi.org/10.3390/electrochem5030018

Academic Editor: Győző G. Lang

Received: 20 May 2024
Revised: 3 July 2024
Accepted: 8 July 2024
Published: 16 July 2024



## 1. Introduction

Electrodeposited nickel (Ni) and Ni-based alloys have garnered significant interest due to their excellent mechanical, electrical, and thermal properties [1,2], which make them suitable for a wide range of applications, including electronics, microelectromechanical systems (MEMS), and protective coatings [3,4]. The increasing demand for miniaturized electronic devices and components necessitates a deeper understanding of the micro-mechanical properties of these materials, as the mechanical performance at the microscale can significantly differ from the bulk properties. Ni-based alloys, such as Ni–P [5], Ni–B [6], Ni–W [7], and Ni–Co [8] are particularly notable for their enhanced properties compared with pure nickel. These enhancements are primarily attributed to the incorporation of alloying elements like phosphorus (P), boron (B), tungsten (W), and cobalt (Co), which can influence the crystallographic structure and precipitate formation, thereby affecting the mechanical strength, hardness, and thermal stability of the alloys. Among these, Ni–W alloys stand out for their exceptional qualities, including high wear resistance, superior hardness, and excellent corrosion resistance [9–11]. These attributes make Ni–W alloys highly suitable for a variety of demanding applications.

Electrodeposition is a convenient method to fabricate complex geometries, including intricate structures and cavities, for specific applications such as micro-components in

MEMS devices [12,13]. By precisely adjusting the electrodeposition parameters, properties of the Ni–W alloy can be adjusted to meet the needs of applications.

Electrodeposition is often conducted using the direct constant current (DC) method [14]. Although the DC method is simple and allows the control of thickness during the deposition time, it is important to note limitations associated with this technique [15], specifically lack of control of the side reactions leads to defective results [7,16–22] caused by the adsorbed hydrogen gas bubbles [23], high internal stress [21,22,24], or hydrogen embrittlement [16]. The reduction potential of Ni is less noble than that of hydrogen reduction. This makes hydrogen reduction an inevitable side reaction in the electrodeposition of Ni-based materials. The reduced hydrogen could form hydrogen gas bubbles and adsorb onto the electrode surface to form defects on the surfaces of the electrodeposited material. Also, the reduced hydrogen could become interstitial elements in the electrodeposited material, resulting in hydrogen embrittlement, and this is a main cause for the formation of cracks in electrodeposited materials. The high internal stress commonly observed in electrodeposited Ni-based materials is another common cause of cracks.

The utilization of anodic or reversed pulse is an effective strategy to manipulate the local concentration of reactive species near the electrode and the properties of the electrodeposited material [7,17,19]. Specifically, the PRE method involves applying a cathodic (forward) current to the electrode for a predetermined time, followed by an anodic (reverse) current for a relatively short duration. The reverse current induces the discharge of the double layer and initiates the rapid reorganization of ions in the solution [17,18]. This reconfiguration process efficiently addresses various causes of defects, including localized pH changes, hydrogen-induced embrittlement, the production or co-deposition of hydrides and oxides, and concerns related to compositional variability [7]. In addition, the pulse reverse method helps to address problems such as hydrogen evolution and localized pH changes, which can have a negative effect on film quality. By reducing internal stresses and improving overall smoothness, the pulse reverse technique promotes a more uniform microstructure and decreases residual stresses within the film. As a result, the PRE method is an extremely effective strategy for minimizing the impact of side reactions, leading to the production of electrodeposited materials that are free from defects and have improved mechanical properties.

The assessment of mechanical properties of electrodeposited film-like materials can be conveniently carried out via hardness tests [25,26]. The determination of hardness involves assessing the indentation produced on the surfaces of the electrodeposited film following the application of a consistent load for a specific duration. The hardness is then determined by calculating the indentation size and the applied loading force. The term used to describe the level of hardness is referred to as micro-hardness [25] or nano-hardness [26], depending on whether the indentation size is measured in micrometers or nanometers, respectively.

In a study on the micro-hardness of electrodeposited Ni–W alloys [19], the W content is increased following an increase in the pulse current density, and the increased W content results higher micro-hardness in the Ni–W alloys. Nevertheless, it is worth noting that it is difficult to eliminate influences from the substrate beneath the Ni–W layer on the formation of the indentation mark, even for nano-hardness tests [20]. Also, the mechanical properties of metallic materials are reported to be dependent on the size of the sample used in the assessment of mechanical properties, and this is known as the sample size effect [27].

The micro-compression test was developed to accurately evaluate the mechanical properties of micro-scale samples for applications in miniaturized electronic systems [27–30]. Previous studies have investigated the micro-mechanical properties of pure nickel composed of micro-grains [28] and nano-grains [29], Ni–B alloys [27], and Ni–P alloys [30]. However, research on the micro-mechanical properties of Ni–W alloys is limited, yet its properties, such as hardness, yield strength, and ductility, are crucial for the design and performance of micro-components.

The primary objective of this research is to investigate the influence of pulse reverse time and forward current densities on the PRE of Ni–W alloys, as well as to investigate

the mechanical properties of electrodeposited Ni–W alloys. The mechanical properties are evaluated via a micro-Vickers hardness test and micro-compression tests using non-tapered micro-pillar type specimens manufactured from the electrodeposited Ni–W alloys.

## 2. Materials and Methods

### *2.1. Ni–W Alloy Electrodeposition*

Ni–W alloy electrodeposition was conducted with a two-electrode system. The counter electrode employed was a 99.95% platinum plate (Kikuya PM Co., Ltd., Tokyo, Japan), with a surface area of 4 $cm^2$ in contact with the electrolyte. Briefly, 99.96% copper plates (Kikuya PM Co., Ltd., Tokyo, Japan) were used as the substrate for the working electrode, and the exposed surface area was defined at 1 $cm^2$. Prior to electrodeposition, the substrates underwent pretreatment in 0.1 M sulfuric acid for 1 minute at room temperature to eliminate surface oxides. Alloy electrodeposition was carried out at a temperature of 65 °C using a commercially available Ni–W alloy electrolyte provided by MATSUDA SANGYO Co., Ltd., Tokyo, Japan. The composition was 6.0% $Na_2WO_4$-$2H_2O$ and 2.4% $NiSO_4$-$6H_2O$. Sulfuric acid and ammonia were utilized for pH adjustments to the electrolyte. The electrolyte was constantly mixed by stirring it at 600 rpm using a cross-shape magnetic stirrer.

The electrodeposition process was carried out using the DC and PRE methods. For the DC method, a forward (cathodic) current density of 50 mA/$cm^2$ was applied for 4800 s to give a total charge density of 240 C/$cm^2$. For the PRC method, the forward (cathodic) current density was 30 mA/$cm^2$, 50 mA/$cm^2$, or 70 mA/$cm^2$, and the time was either 66.7 s or 40.0 s or 28.6 s, respectively, to ensure a charge density of 2 C/$cm^2$ in one cycle of the forward pulse. A constant reverse (anodic) current density of −5 mA/$cm^2$ was used for 1.5 s. A graphical representation of one cycle of the forward reverse current is illustrated in Figure 1. In total, 120 cycles of the forward reverse current were run to give a total charge density of roughly 240 C/$cm^2$.

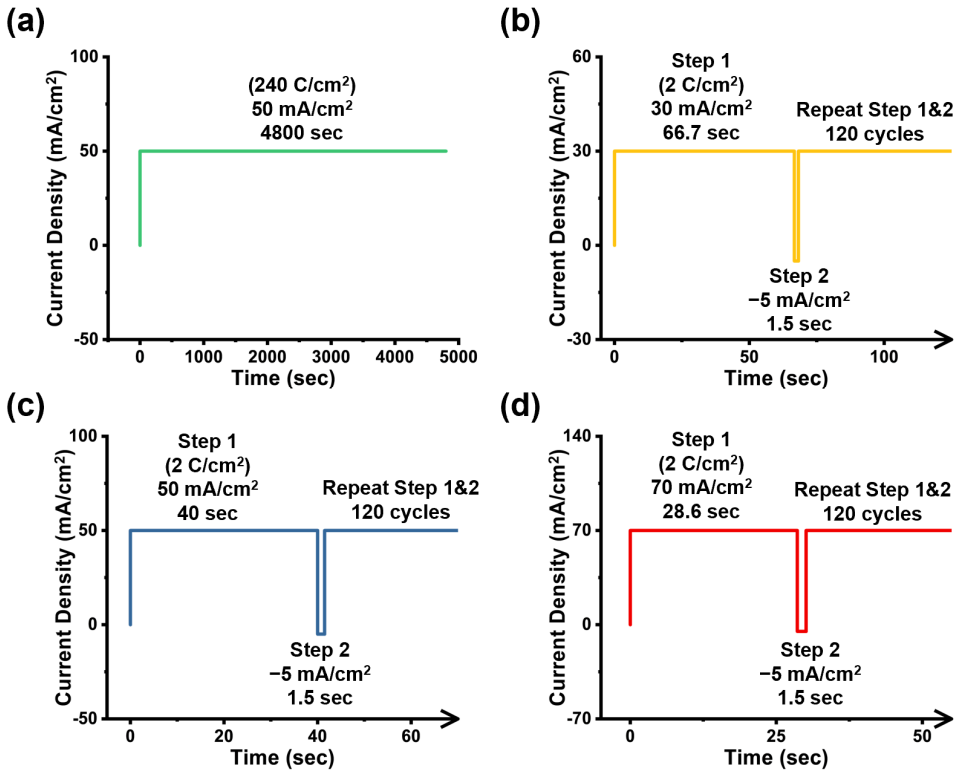


**Figure 1.** The representation of the electrodeposition methods. (**a**) The DC method and the PRE method at different forward current densities: (**b**) 30 mA/$cm^2$, (**c**) 50 mA/$cm^2$, and (**d**) 70 mA/$cm^2$.

To enhance understanding, Scheme 1 represents the Ni–W electrodeposition mechanism. This figure illustrates the electrolysis process, highlighting the formation of hydrogen gas and its subsequent impact on the Ni–W film formation on the copper base. The schematic addresses the primary challenges associated with Ni–W electrodeposition, particularly the formation of voids and cracks due to the electrolysis of water as a side reaction. The main cause of crack formation is the residual tensile stress generated by hydrogen reduction at the cathode surface. Specifically, hydrogen diffuses into the Ni–W lattice, causing lattice expansion. Since hydrogen cannot remain dissolved within the Ni-W film, it diffuses out based on its diffusion and solubility coefficients. Consequently, the expulsion of hydrogen from the Ni–W lattice creates residual tensile stress, leading to contraction and eventual crack formation.

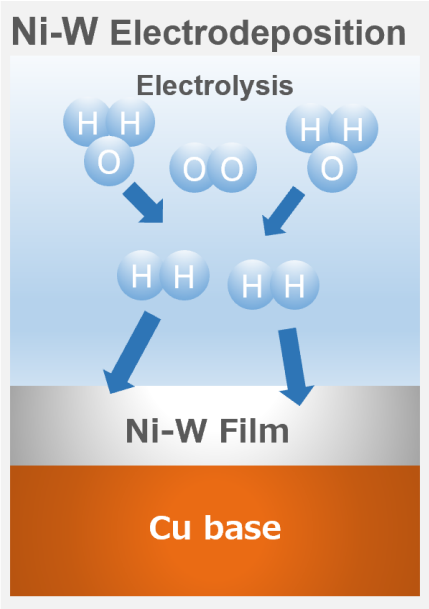


**Scheme 1.** Ni–W electrodeposition process and impact of hydrogen evolution.

### *2.2. Characterization*

The crystalline properties of the Ni–W alloy were examined using an X-ray diffractometer (XRD, Ultima IV, Rigaku Corp., Tokyo, Japan) with a scanning rate of 0.04° per second. Surface morphology was examined using a scanning electron microscope (SEM, SU4300SE, Hitachi Co., Ltd., Tokyo, Japan). The elemental composition was determined through energy-dispersive X-ray spectroscopy (EDS, EMAX EX-250, Horiba Co., Ltd., Kyoto, Japan) integrated with the SEM, with an estimated error of ± 2% in the at% of W content. Mechanical properties were assessed using Vickers micro-hardness tests with a load of 0.025 kg, performed using Micro Vickers Hardness Testing Machine (HMV-G20S, Shimadzu Corp., Kyoto, Japan). The Faradaic efficiency (FE) was calculated using the following equation:

$$\mathrm{FE} = \frac{m}{Q_{\mathrm{total}}} \sum \frac{C_i n_i F}{\mathrm{MW}_i} \times 100\% \quad (1)$$

where $m$ is the measured mass of the electrodeposited Ni–W alloy, $Q_{\mathrm{total}}$ is the total charge (240 C in this study), $C_i$ is the weight fraction of the element (Ni or W) determined by the EDS, $n_i$ is the number of electrons involved in the reduction of the specific element (2 for Ni and 6 for W), $F$ is the Faraday constant (96,485 C/mol), and $\mathrm{MW}_i$ is the molecular weight for the specific element.

### *2.3. Fabrication of Micro-Pillar and Micro-Compression Test*

The micro-pillars were meticulously prepared from the electrodeposited Ni–W alloys using a focused ion beam system (FIB, FB2100, Hitachi, Tokyo, Japan). The fabrication process is illustrated in Figure 2. To achieve precise dimensions [28,29], a four-step milling approach with varied beam currents was employed. Coarse milling utilized beam currents of 6.64 nA, 1.48 nA, and 0.35 nA, while fine milling and final polishing were conducted at 0.07 nA. The resulting micro-pillars had a square cross-section of 10 μm × 10 μm and a height of 20 μm. The micro-pillars were characterized using a scanning ion microscope (SIM) integrated into the FIB system, both before and after the micro-compression test.

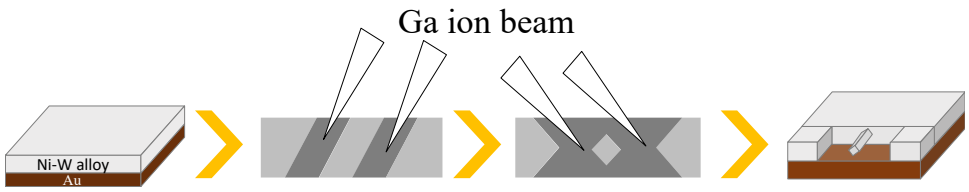


**Figure 2.** Illustration of the micro-pillar fabrication procedures.

Figure 3 presents the micro-testing machine developed within our research group. This apparatus featured a flat-tipped indenter with a 50 μm diameter on its upper surface. With a load resolution of 10 μN and a displacement resolution of 5 nm, all micro-compression tests were conducted at a constant displacement rate of 0.1 μm/s, resulting in a constant strain rate of $5 \times 10^{-3}$ $s^{-1}$.

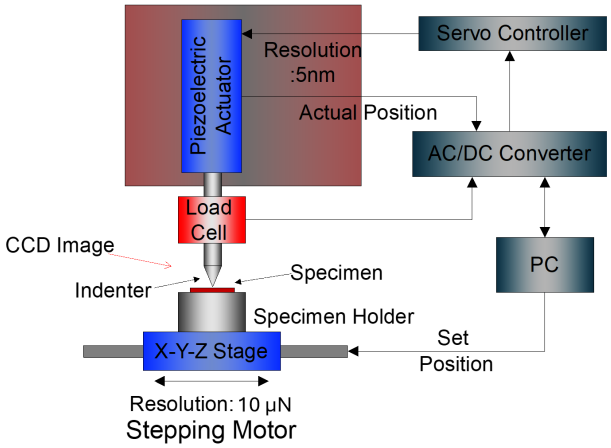


**Figure 3.** Micro-mechanical test systems developed in our group.

## 3. Results and Discussion

The surface conditions of the Ni–W alloys prepared via the DC and PRE methods were examined through SEM images, as shown in Figure 4. In Figure 4a, the DC Ni–W alloy displayed noticeable cracks and voids on the surface. The cracks are believed to be attributable to internal stress [24]. Furthermore, delamination of the Ni–W alloy from the substrate was observed, which is also suggested to be caused by the internal stress. The presence of hydrogen gas bubbles on the electrode surface is thought to be the underlying cause of the voids. Conversely, Figure 4b illustrates the surface of the PRC Ni–W alloy, produced using a forward current density of 50 mA/cm$^2$, which appears uniform, with an absence of cracks and voids. This indicates that the PRE method, particularly the application of a reverse current, effectively improves the surface conditions of the electrodeposited Ni–W alloy. When the forward current density was increased to 70 mA/cm$^2$, as shown in Figure 4c, although no voids were present, the surface exhibited rougher conditions and cracks. The observed cracks are likely attributed to increased internal stress resulting from the use of a higher current density [24]. Interestingly, when the forward current density

was reduced to 30 mA/cm$^2$, as shown in Figure 4d, the surface condition was similar to that of the PRE 50 mA/cm$^2$ sample, with the exception of crack formation. The potential cause of these cracks will be discussed in a subsequent section.

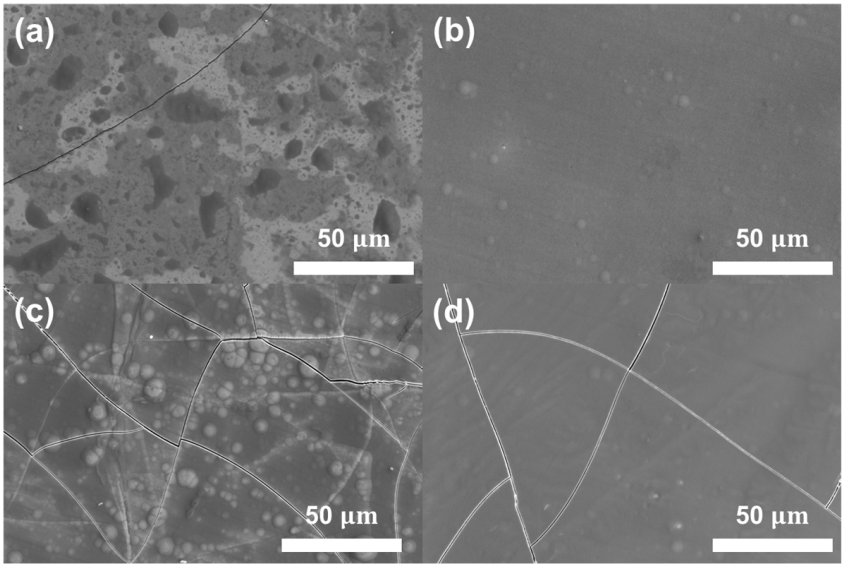


**Figure 4.** SEM images of the Ni–W alloy prepared via the (**a**) DC method at 50 mA/cm$^2$ and via the PRE method at (**b**) 50 mA/cm$^2$, (**c**) 70 mA/cm$^2$, and (**d**) 30 mA/cm$^2$.

The DC Ni–W alloy exhibited a W content of 20.2 at%, while the W content was 20.1 at% in the PRE Ni–W alloy prepared with a forward current density of 50 mA/cm$^2$. This marginal variation in the W content suggests that the reverse current did not significantly alter the composition. On the other hand, with an increase in the forward current density from 30 mA/cm$^2$ to 70 mA/cm$^2$, there was an increase in the W content, as shown in Table 1. This increasing trend of the W content following an increase in the forward current density is the same as that reported in a previous study [11]. The FE decreased from 50.1% at 30 mA/cm$^2$ to 45.7% at 70 mA/cm$^2$ as the forward current density increased. The decrease in the FE at higher forward current densities can be ascribed to the promoted side reactions, such as the hydrogen evolution reaction.

**Table 1.** Properties of the Ni–W alloys prepared via the PRE method.

| Forward Current Density (mA/cm$^2$) | W Content (at%) | FE (%) | Grain Size (nm) | Thickness (µm) |
|---|---|---|---|---|
| 30 | 18.2 ± 2.0 | 50.1 | 9.0 | 39.1 |
| 50 | 20.1 ± 2.0 | 49.0 | 11.8 | 35.1 |
| 70 | 21.6 ± 2.0 | 45.7 | 13.7 | 27.6 |

The XRD patterns of the Ni–W alloy synthesized in this study revealed distinct peaks corresponding to the (111), (200), and (220) crystal planes of a face-centered cubic (FCC) structure, as illustrated in Figure 5a. Notably, the XRD peak intensity of (111) was the most prominent among all the observed peaks. Furthermore, a comparison with the XRD pattern of pure nickel showed a noticeable shift of the Ni–W peaks towards lower 2θ angles. Specifically, based on JCPDS No. 04-0850, the peaks for pure nickel are located at 2θ = 44.4°, 51.8°, and 76.4°, whereas the Ni–W peaks appear at lower angles. This observed ~5° shift in the high-number facet is significant and indicates the formation of a tungsten (W) solid solution ($\alpha$-Ni(W)) within the FCC nickel (Ni) matrix, resulting in an expansion of the nickel lattice due to tungsten dissolution [31]. The reference angles provided by the JCPDS database are based on pure nickel, and in our study, the incorporation of W atoms into the

Ni lattice caused an expansion due to the larger atomic radius of W compared with that of Ni. This expansion led to a shift in the XRD peaks towards lower 2θ angles. Similar shifts have been reported in the literature, including the study by Sriraman et al. [32], which supports our observations. The average grain size of the alloy was estimated using the Scherrer equation based on the (111) XRD peak [33,34]. The results presented in Figure 5b indicate that as the forward current density increased, the average grain size grew from 9.0 nm at 30 mA/cm$^2$ to 11.8 nm at 50 mA/cm$^2$, and further to 13.7 nm at 70 mA/cm$^2$.

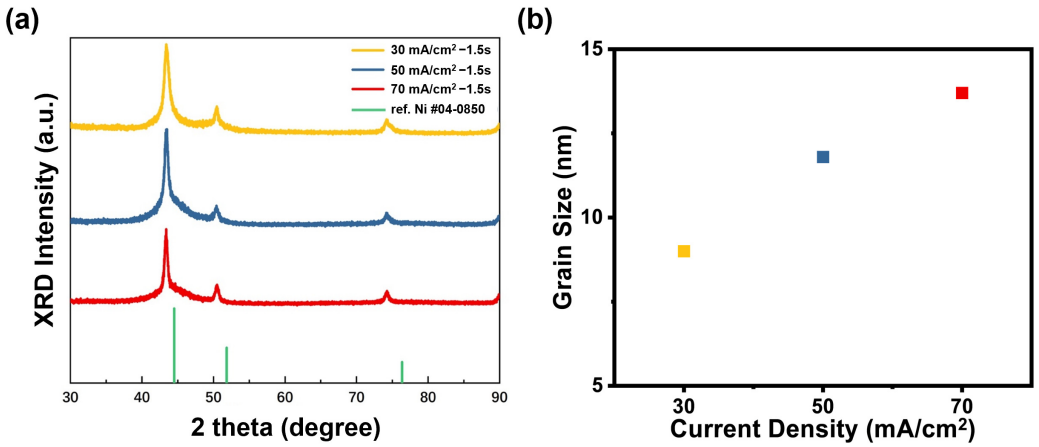


**Figure 5.** (**a**) XRD patterns of the Ni–W alloys prepared using the PRE method. (**b**) Average grain size at different current densities.

An increase in the current density typically leads to an increase in the nuclei density and a grain refinement effect. However, when side reactions become more significant with an increase in the current density, the grain coarsening effect may occur [35]. In this study, the trends observed in the FE and the average grain size are consistent with each other. The forward current density increase resulted in a decrease in the FE, indicating promoted side reactions, which eventually led to the grain coarsening effect.

In addition, the finest average grain size was observed in the PRE 30 mA/cm$^2$ sample. Refinement of the average grain size in electrodeposited materials is another cause of internal stress that could lead to the formation of cracks. This ultrafine grains are suggested to be the cause of the cracks observed in the PRE 30 mA/cm$^2$ sample.

The thickness of the electrodeposited Ni–W alloys was evaluated via observations of the cross-sections. The thickness reduced from 39.1 μm to 27.6 μm as the forward current density increased from 30 mA/cm$^2$ to 70 mA/cm$^2$. The total charge density applied to the three PRE Ni–W alloys were the same. This change in the thickness corresponds well with the FE; a low FE resulted in reduced thickness.

The mechanical properties were first evaluated using Vickers micro-hardness tests for comparisons with the results of the micro-compression tests. However, as can be seen in Figure 6, the development of cracks around the indentation site is evident. It is believed that these cracks were caused by the high internal stresses generated when using high forward current densities. This compromises the reliability of the micro-hardness measurements because the cracks disrupted the uniform load distribution, reduced structural integrity around the indents, and caused instability in the indentation geometry. Consequently, to obtain more reliable and accurate measurements, mechanical properties were assessed using micro-compression tests instead. This method minimizes the influence of surface defects and provides a controlled environment in which to measure a material's stress–strain response directly.

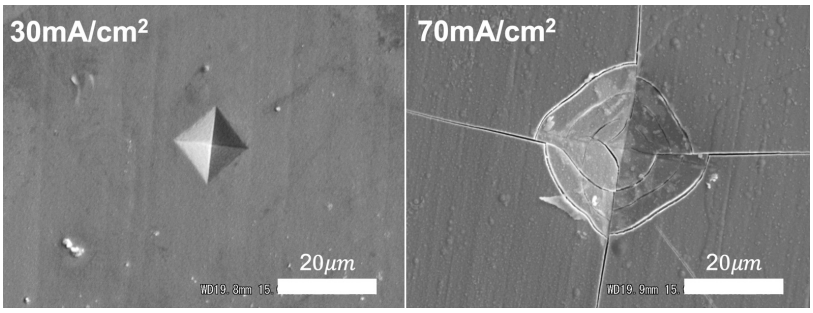


**Figure 6.** SEM images of the Ni–W alloys fabricated via the PRE method after the micro-hardness test.

Figure 7 presents images of the micro-pillars before and after the micro-compression test, which were fabricated from Ni–W alloys prepared using the PRE method. Following the micro-compression test, all micro-pillars exhibited plastic deformation, indicating the occurrence of yield. The stress–strain (SS) curves derived from the micro-compression tests are provided in Figure 8. The yield points, indicating the boundary between the elastic and plastic deformation regions, were not well defined among the three SS curves. Therefore, the yield stress was determined at the intersection point of the SS curve with the 0.2% offset line in the elastic deformation region. The micro-pillars fabricated with the Ni–W alloy electrodeposited at a forward current density of 70 mA/cm$^2$ exhibited the highest yield stress, measuring 3071 MPa. The micro-pillars produced with forward current densities of 30 mA/cm$^2$ and 50 mA/cm$^2$ had yield stresses of 2753 MPa and 2948 MPa, respectively.

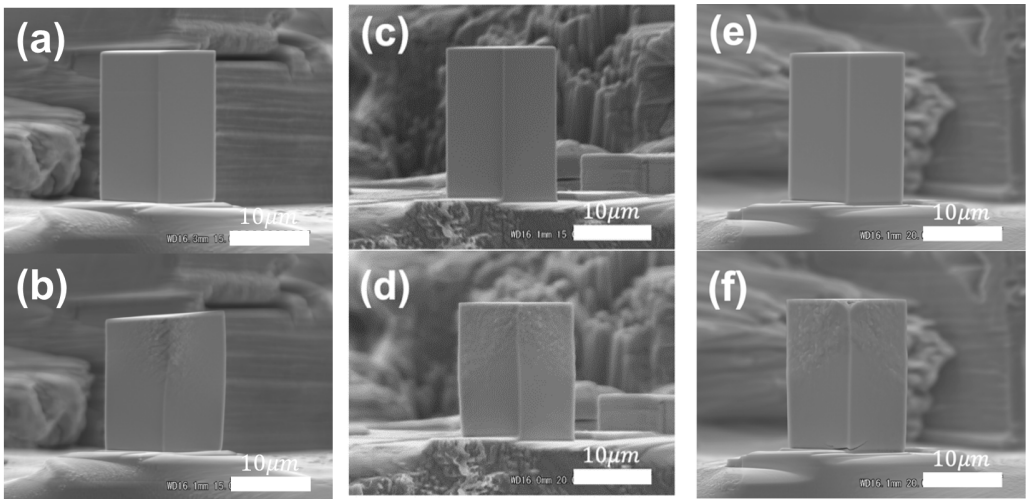


**Figure 7.** SIM images of the PRE 30 mA/cm$^2$ micro-pillar (**a**) before and (**b**) after the compression test, the 50 mA/cm$^2$ micro-pillar (**c**) before and (**d**) after the compression test, and the 70 mA/cm$^2$ (**e**) before and (**f**) after the compression test.

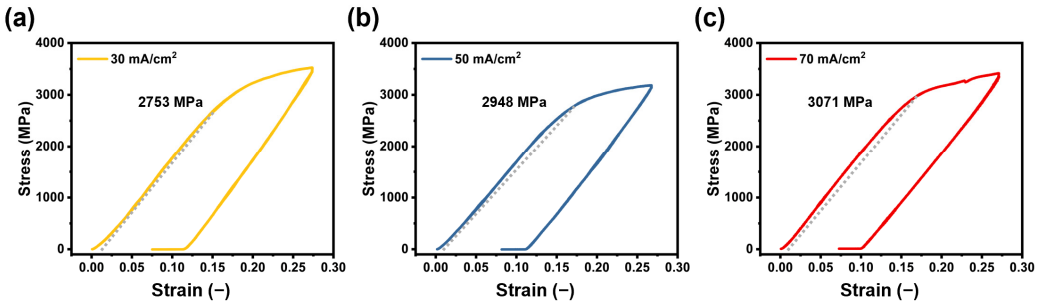


**Figure 8.** Stress–strain curves of the (**a**) 30, (**b**) 50, and (**c**) 70 mA/cm$^2$ micro-pillars.

The mechanical strength of Ni–W alloys is influenced by both grain boundary strengthening and solid solution strengthening, attributed to the fine average grain size and tungsten content, respectively. In our study, the PRE 30 mA/cm$^2$ sample exhibited the finest average grain size of 9.0 nm, which would typically result in higher yield strength due to grain boundary strengthening. This mechanism, known as the Hall–Petch relationship, suggests that smaller grains provide a greater grain boundary area, thereby impeding dislocation movement and enhancing strength. However, the highest yield stress was observed in the PRE 70 mA/cm$^2$ sample, which had an average grain size of 13.7 nm. This can be explained by the significant role of solid solution strengthening at higher current densities. At 70 mA/cm$^2$, the incorporation of tungsten atoms into the nickel matrix was maximized, creating more lattice distortions. These distortions hinder dislocation movement more effectively than grain boundaries alone, leading to enhanced yield stress. Therefore, while grain size is an important factor in determining mechanical strength, the composition and extent of solid solution strengthening are crucial [36,37]. The increased tungsten content in the PRE 70 mA/cm$^2$ sample provided significant solid solution strengthening, which outweighed the grain boundary strengthening effect seen in the PRE 30 mA/cm$^2$ sample. This indicates that solid solution strengthening, due to the increased incorporation of tungsten atoms, plays a more significant role in determining the yield stress in the Ni–W alloys evaluated in this study.

## 4. Conclusions

Electrodeposited Ni–W alloys were prepared using the PRE method, and the effects of the forward current density on their properties were investigated. At a forward current density of 50 mA/cm$^2$, the surface of the electrodeposited Ni–W alloy showed improved smoothness with no cracks and reached a thickness of 35.1 μm. As the forward current density increased, the W content and average grain size also increased. At 70 mA/cm$^2$, the W content was 21.6 at% and the average grain size was 13.7 nm. The micro-pillar prepared from the sample with a forward current density of 70 mA/cm$^2$ exhibited the highest yield stress at 3071 MPa, mainly due to the solid solution mechanism.

In conclusion, the pulsed reverse electrodeposition method effectively enhances the surface smoothness and mechanical properties of Ni–W alloys. The optimized forward current density of 50 mA/cm$^2$ offers a balance between surface quality and mechanical performance, making it suitable for applications in miniaturized electronic components. However, the highest yield stress was observed at 70 mA/cm$^2$ due to the increased tungsten content and solid solution strengthening. Overall, the PRE method shows significant potential for preparing defect-free, high-performance materials for MEMS components and other advanced micro-electronic applications.

**Author Contributions:** Conceptualization, Z.G.; methodology, Z.G. and Y.J.; validation, J.-Y.W., Y.J., T.K., and C.-Y.C.; formal analysis, Z.G.; investigation, Z.G.; resources, H.-E.L., X.L. and D.Y.; data curation, Z.G.; writing—original draft preparation, Z.G.; writing—review and editing, J.-Y.W.; visualization, Z.G., J.-Y.W.; supervision, T.-F.M.C.; project administration, M.S. and T.-F.M.C.; funding acquisition, M.S. and T.-F.M.C. All authors have read and agreed to the published version of the manuscript.

**Funding:** This work was supported by the Research Center for Biomedical Engineering, Tokyo Institute of Technology, and JSPS KAKENHI, Grant Number JP21H01668.

**Institutional Review Board Statement:** Not applicable.

**Informed Consent Statement:** Not applicable.

**Data Availability Statement:** The data presented in this study are available on request from the corresponding author.

**Conflicts of Interest:** The authors declare that the research was conducted in the absence of any commercial or financial relationships that could be construed as a potential conflict of interest.

## References


1. Oriňáková, R.; Turoňová, A.; Kladeková, D.; Gálová, M.; Smith, R.M. Recent Developments in the Electrodeposition of Nickel and Some Nickel-Based Alloys. *J. Appl. Electrochem.* **2006**, *36*, 957–972. [CrossRef]
2. Saini, A.; Singh, G.; Mehta, S.; Singh, H.; Dixit, S. A Review on Mechanical Behaviour of Electrodeposited Ni-Composite Coatings. *Int. J. Interact. Des. Manuf. (IJIDeM)* **2023**, *17*, 2247–2258. [CrossRef]
3. Rai, P.K.; Gupta, A. Investigation of Surface Characteristics and Effect of Electrodeposition Parameters on Nickel-Based Composite Coating. *Mater. Today Proc.* **2021**, *44*, 1079–1085. [CrossRef]
4. Mahidashti, Z.; Aliofkhazraei, M.; Lotfi, N. Review of Nickel-Based Electrodeposited Tribo-Coatings. *Trans. Indian Inst. Met.* **2018**, *71*, 257–295. [CrossRef]
5. Lelevic, A.; Walsh, F.C. Electrodeposition of NiP Alloy Coatings: A Review. *Surf. Coat. Technol.* **2019**, *369*, 198–220. [CrossRef]
6. Ünal, E.; Yaşar, A.; Karahan, İ.H. A Review of Electrodeposited Composite Coatings with Ni–B Alloy Matrix. *Mater. Res. Express* **2019**, *6*, 092004. [CrossRef]
7. Allahyarzadeh, M.H.; Aliofkhazraei, M.; Rezvanian, A.R.; Torabinejad, V.; Sabour Rouhaghdam, A.R. Ni-W Electrodeposited Coatings: Characterization, Properties and Applications. *Surf. Coat. Technol.* **2016**, *307*, 978–1010. [CrossRef]
8. Karimzadeh, A.; Aliofkhazraei, M.; Walsh, F.C. A Review of Electrodeposited Ni-Co Alloy and Composite Coatings: Microstructure, Properties and Applications. *Surf. Coat. Technol.* **2019**, *372*, 463–498. [CrossRef]
9. Jones, A.R.; Hamann, J.; Lund, A.; Schuh, C. Nanocrystalline Ni-W Alloy Coating for Engineering Applications. *Plat. Surf. Finish.* **2010**, *97*, 52–60.
10. Wasekar, N.P.; Sundararajan, G. Sliding Wear Behavior of Electrodeposited Ni–W Alloy and Hard Chrome Coatings. *Wear* **2015**, *342–343*, 340–348. [CrossRef]
11. Kumar, K.A.; Kalaignan, G.P.; Muralidharan, V.S. Pulse Electrodeposition and Characterization of Nano Ni–W Alloy Deposits. *Appl. Surf. Sci.* **2012**, *259*, 231–237. [CrossRef]
12. Larson, C.; Farr, J.P.G. Current Research and Potential Applications for Pulsed Current Electrodeposition–A Review. *Trans. IMF* **2012**, *90*, 20–29. [CrossRef]
13. Slavcheva, E.; Mokwa, W.; Schnakenberg, U. Electrodeposition and Properties of NiW Films for MEMS Application. *Electrochim. Acta* **2005**, *50*, 5573–5580. [CrossRef]
14. Xiao, F.; Hangarter, C.; Yoo, B.; Rheem, Y.; Lee, K.-H.; Myung, N.V. Recent Progress in Electrodeposition of Thermoelectric Thin Films and Nanostructures. *Electrochim. Acta* **2008**, *53*, 8103–8117. [CrossRef]
15. Walsh, F.C.; Wang, S.; Zhou, N. The Electrodeposition of Composite Coatings: Diversity, Applications and Challenges. *Curr. Opin. Electrochem.* **2020**, *20*, 8–19. [CrossRef]
16. Hillier, E.M.K.; Robinson, M.J. Permeation Measurements to Study Hydrogen Uptake by Steel Electroplated with Zinc–Cobalt Alloys. *Corros. Sci.* **2006**, *48*, 1019–1035. [CrossRef]
17. Chandrasekar, M.S.; Pushpavanam, M. Pulse and Pulse Reverse Plating—Conceptual, Advantages and Applications. *Electrochim. Acta* **2008**, *53*, 3313–3322. [CrossRef]
18. Ahmad, Y.H.; Mohamed, A.M.A. Electrodeposition of Nanostructured Nickel-Ceramic Composite Coatings: A Review. *Int. J. Electrochem. Sci.* **2014**, *9*, 1942–1963. [CrossRef]
19. Hou, K.-H.; Chen, Y.-C. Preparation and Wear Resistance of Pulse Electrodeposited Ni–W/$Al_2O_3$ Composite Coatings. *Appl. Surf. Sci.* **2011**, *257*, 6340–6346. [CrossRef]
20. Manika, I.; Maniks, J. Effect of Substrate Hardness and Film Structure on Indentation Depth Criteria for Film Hardness Testing. *J. Phys. D Appl. Phys.* **2008**, *41*, 074010. [CrossRef]
21. Nguyen, V.C.; Lee, C.Y.; Chen, F.J.; Lin, C.S.; Liu, T.Y. Study on the Internal Stress of Nickel Coating Electrodeposited in an Electrolyte Mixed with Supercritical Carbon Dioxide. *Surf. Coat. Technol.* **2012**, *206*, 3201–3207. [CrossRef]
22. Lin, C.S.; Lee, C.Y.; Chen, F.J.; Li, W.C. Structural Evolution and Internal Stress of Nickel-Phosphorus Electrodeposits. *J. Electrochem. Soc.* **2005**, *152*, C370. [CrossRef]
23. Besra, L.; Uchikoshi, T.; Suzuki, T.S.; Sakka, Y. Application of Constant Current Pulse to Suppress Bubble Incorporation and Control Deposit Morphology during Aqueous Electrophoretic Deposition (EPD). *J. Eur. Ceram. Soc.* **2009**, *29*, 1837–1845. [CrossRef]
24. Abadias, G.; Chason, E.; Keckes, J.; Sebastiani, M.; Thompson, G.B.; Barthel, E.; Doll, G.L.; Murray, C.E.; Stoessel, C.H.; Martinu, L. Review Article: Stress in Thin Films and Coatings: Current Status, Challenges, and Prospects. *J. Vac. Sci. Technol. A* **2018**, *36*, 020801. [CrossRef]
25. Ogihara, H.; Wang, H.; Saji, T. Electrodeposition of Ni–B/SiC Composite Films with High Hardness and Wear Resistance. *Appl. Surf. Sci.* **2014**, *296*, 108–113. [CrossRef]
26. Valova, E.; Armyanov, S.; Franquet, A.; Petrov, K.; Kovacheva, D.; Dille, J.; Delplancke, J.-L.; Hubin, A.; Steenhaut, O.; Vereecken, J. Comparison of the Structure and Chemical Composition of Crystalline and Amorphous Electroless Ni-W-P Coatings. *J. Electrochem. Soc.* **2004**, *151*, C385. [CrossRef]
27. Jiang, Y.; Chen, C.-Y.; Kurioka, T.; Luo, X.; Yamane, D.; Mizoguchi, M.; Kudo, O.; Maeda, R.; Sone, M.; Chang, T.-F.M. Specimen Size Effect on the Strength of Nickel-Boron Alloys. *Mater. Lett.* **2023**, *349*, 134742. [CrossRef]

28. Yamamoto, T.; Igawa, K.; Tang, H.; Chen, C.-Y.; Chang, T.-F.M.; Nagoshi, T.; Kudo, O.; Maeda, R.; Sone, M. Effects of Current Density on Mechanical Properties of Electroplated Nickel with High Speed Sulfamate Bath. *Microelectron. Eng.* **2019**, *213*, 18–23. [CrossRef]
29. Nagoshi, T.; Chang, T.-F.M.; Tatsuo, S.; Sone, M. Mechanical Properties of Nickel Fabricated by Electroplating with Supercritical $CO_2$ Emulsion Evaluated by Micro-Compression Test Using Non-Tapered Micro-Sized Pillar. *Microelectron. Eng.* **2013**, *110*, 270–273. [CrossRef]
30. Hotta, T.; Chang, T.-F.M.; Chen, C.-Y.; Sawae, H.; Imada, Y.; Mizoguchi, M.; Kudo, O.; Maeda, R.; Sone, M. Micro-Compression Characterization and Thermal Stability of Electrolessly Plated Nickel Phosphorus Alloy. *ECS J. Solid State Sci. Technol.* **2021**, *10*, 035007. [CrossRef]
31. Kumar, U.P.; Shanmugan, S.; Kennady, C.J.; Shibli, S.M.A. Anti-Corrosion and Microstructural Properties of Ni–W Alloy Coatings: Effect of 3,4-Dihydroxybenzaldehyde. *Heliyon* **2019**, *5*, E01288. [CrossRef] [PubMed]
32. Sriraman, K.R.; Raman, S.G.S.; Seshadri, S.K. Corrosion Behaviour of Electrodeposited Nanocrystalline Ni–W and Ni–Fe–W Alloys. *Mater. Sci. Eng. A* **2007**, *460–461*, 39–45. [CrossRef]
33. Patterson, A.L. The Scherrer Formula for X-ray Particle Size Determination. *Phys. Rev.* **1939**, *56*, 978. [CrossRef]
34. He, K.; Chen, N.; Wang, C.; Wei, L.; Chen, J. Method for Determining Crystal Grain Size by X-ray Diffraction. *Cryst. Res. Technol.* **2018**, *53*, 1700157. [CrossRef]
35. Guo, J.D.; Wang, X.L.; Dai, W.B. Microstructure Evolution in Metals Induced by High Density Electric Current Pulses. *Mater. Sci. Technol.* **2015**, *31*, 1545–1554. [CrossRef]
36. Rupert, T.J.; Trenkle, J.C.; Schuh, C.A. Enhanced Solid Solution Effects on the Strength of Nanocrystalline Alloys. *Acta Mater.* **2011**, *59*, 1619–1631. [CrossRef]
37. Schuh, C.A.; Nieh, T.G.; Iwasaki, H. The Effect of Solid Solution W Additions on the Mechanical Properties of Nanocrystalline Ni. *Acta Mater.* **2003**, *51*, 431–443. [CrossRef]